Biocatalysis and Agricultural Biotechnology 19 (2019) 101175

Contents lists available at ScienceDirect

Biocatalysis and Agricultural Biotechnology

journal homepage: www.elsevier.com/locate/bab

Isorhamnetin encapsulation into biogenic silica from *Cyclotella* sp. using a microfluidic device for drug delivery applications

Elena I. Mancera-Andrade[a], Ali Parsaeimehr[a,b], Federico Ruiz-Ruiz[a], Gregory L. Rorrer[c], José González-Valdez[a], Hafiz M.N. Iqbal[a,*], Roberto Parra-Saldivar[a,d,**]

[a] Tecnologico de Monterrey, School of Engineering and Sciences, Campus Monterrey, Ave. Eugenio Garza Sada 2501, Monterrey, NL, CP 64849, Mexico
[b] University of Florida, Citrus Research and Education Center, 700 Experiment Station Road, Lake Alfred, FL, 33850, United States
[c] School of Chemical, Biological, and Environmental Engineering, Oregon State University, Corvallis, OR, United States
[d] School of Chemical and Biomedical Engineering, College of Engineering, Nanyang Technological University, 62 Nanyang Drive, Singapore, 637459, Singapore

ARTICLE INFO

Keywords:
Microfluidic device
Biogenic silica
Isorhamnetin
Encapsulation
Drug delivery

ABSTRACT

Diatoms have the peculiarity to synthesize amorphous silica around the cell wall. Frustules (empty silica shells) have the advantages of being biocompatible, biodegradable, nontoxic and rich with hydroxyl groups on the surface. Frustules have been used in diverse fields, but recently their application in the biomedical field has been investigated. Drug delivery systems (DDS) have been studied to improve the therapeutic effect of different drugs, especially hydrophobic drugs. Different encapsulation methodologies have been used to load the drug in a carrier such as drop-wise methodology or solvent evaporation. However, a reproducible methodology that reduces handling error must be explored. Herein, a novel technique ESCARGOT (Embedded SCAffold RemovinG Open Technology) was used to fabricate the microfluidic device and exploited as a novel tool to encapsulate hydrophobic drugs into the in-house developed biogenic silica from *Cyclotella* sp. Isorhamnetin was used as a model drug with hydrophobic in nature. Three different concentrations were studied: 20, 60 and 100 μg/mL, and three different resident times in the device (0.4, 1 and 2 min). The highest encapsulation efficiency (EE%) and loading capacity (LC%) were 17.92% and 1.63% respectively. According to the statistical analysis, the optimum conditions to obtain a maximum EE% were 2 min and 20 μg/mL. The isorhamnetin release behavior was observed with a burst release in the first hour with 48.26%, while the total amount of drug was delivered in 3 h. The feasibility of frustules as carriers and the microfluidic device as a mixer was successfully accessed. This methodology could be used as a standardization technique to obtain reproducible results.

1. Introduction

The high-tech advancements in polymer science offer notable potentialities which led to their exploration as a novel carrier in drug delivery systems (DDS) (Iqbal and Keshavarz, 2018). Drug delivery can be defined as a sustained distribution of drugs in a controlled way at a specific target site (Xin et al., 2016; Raza et al., 2019a). The controlled delivery is achieved by taking advantage of the biochemical characteristics of a drug-loaded carrier and environment of the target site. This also additionally benefits an effective drug exposure which maintains the drug in the tissue for longer times giving, in this way, a broad therapeutic window. The attachment or encapsulation of the drug in a carrier allows the protection of it in the physiological environment (Rasheed et al., 2018; Raza et al., 2019b). The main advantages of encapsulation are the enhancement of sensitivity of tumor tissue to drugs, the increment of the drug solubility, bioavailability, drug stability, prolonged half-life, reduction of dose, and the possibility to include two or more drugs into the same carrier (Dong and Mumper, 2010; Fonseca et al., 2015; Vishnubhakthula et al., 2017).

Wide-ranging materials have been used to encapsulate biomolecules such as metallic materials (Hashemipour and Panahi, 2017), polymeric micelles (Logie et al., 2017), liposomes (Joseph, 2018), nanotubes (Liang et al., 2017), dendrimers (Amreddy et al., 2018), biodegradable materials (Graves et al., 2015; Ruiz-Ruiz et al., 2017), and silica particles (Schultz et al., 2018). From all these, silica (silicon dioxide, SiO_2) has been widely studied due to biocompatibility, biodegradability, chemical stability, capacity to change the chemistry of the surface, and large surface for adsorption processes (Diab et al., 2017; Kumar et al.,

* Corresponding author.
** Corresponding author.
E-mail addresses: hafiz.iqbal@tec.mx (H.M.N. Iqbal), r.parra@tec.mx (R. Parra-Saldivar).

https://doi.org/10.1016/j.bcab.2019.101175
Received 22 March 2019; Received in revised form 10 May 2019; Accepted 24 May 2019
Available online 24 May 2019
1878-8181/

2017; Tian and Guo, 2017). Usually, synthetic particles have been used as a mesoporous silica material (de Jesús Rostro-Alanis et al., 2016). However, the production of these particles involves the use of toxic solvents, difficulty to produce uniform pore size and ordered porosity on the surface (Napierska et al., 2010). Hence, biogenic silica from marine organisms provides no toxicity, uniform pore size, biocompatibility, and biodegradability. Diatoms are being the largest producers of silica in water bodies by representing the 45% of total oceanic primary production (Barsanti and Gualtieri, 2014; Javalkote et al., 2015). Diatoms are photosynthetic eukaryotic microorganisms that have the peculiarity to synthesize amorphous silica around the cell wall. The synthesis is performed in a specialized organelle called silica deposition vesicle (SDV). Silicic ions are transported through the membrane with transmembrane proteins called silicic acid transporters (SAT). Once the silicic ions are deposited, peptides such as long-chain polyamines (LCPA), silaffins and silacidins perform hydrolysis and polymerization reactions in an acidic environment. The amount and type of these peptides differ from each diatom species, and they will dictate the diatom shape either centric or pennate (Zhang et al., 2012). Biogenic silica is obtained after cleaning methodologies to remove organic material are completed. Well-established methodologies that involve oxidation reactions and the use of acids, surfactants, organic solvents such as methanol or ethanol, or thermal treatment have been described (Jeffryes et al., 2008; Gültürk and Güden, 2011; Jiang et al., 2014). Different microencapsulation techniques involve the binding or adsorption through electrostatic forces between the particles and the carrier. Most of the common techniques involve the stirring and evaporation. One of the main advantages of traditional techniques is the constant contact between the drug and the carrier which enhances the adsorption process. Nevertheless, the use of toxic solvents, the difficulty of incorporate hydrophilic drugs (depending on the carrier nature), and a time-consuming process have led to the researchers to look for novel solutions (Hans and Lowman, 2002). Microfluidic-based devices allow to study the behavior of fluids in microchannels. One of the main advantages of these devices is the easiness of creating a wide range of microsystems by changing parameters such as flow rate, solvent concentration, solvent nature, channel size and geometry pattern of the device (Ahmed et al., 2018a, 2018b; Sosa-Hernández et al., 2018). While most of the studies have focused the research on the production of tailor-made micro and nanoparticles; microfluidic devices can be used as mixers and microreactors (Mancera-Andrade et al., 2018). For this study, we hypothesize that the use of a microfluidic device as a mixer can address the drawbacks of the traditional encapsulation methodologies.

The most used methodologies for microfluidic device fabrication are lithography, micro milling, micromachining and mold replication (Khan et al., 2013). However, most of these techniques are expensive, time-consuming and the use of specialized equipment. A novel microfluidic fabrication technique using a 3-D mold called ESCARGOT (Embedded SCAffold RemovinG Open Technology) was developed (Saggiomo and Velders, 2015). It involves the use of a 3-D mold of acrylonitrile butadiene styrene (ABS) polymer, that is immersed in polydimethylsiloxane (PDMS), once the PDMS is cured (solidified), the mold is dissolved using acetone. One of the main advantages of this technique is the possible standardization and reproducible process for the fabrication because nowadays 3-D printers are widely used, and the freedom to choose and design the best geometry pattern for the device.

On the other hand, PDMS has been widely used for biomedical applications due to their excellent characteristics such as gas permeability, optical transparency, and chemistry change of the surface with functional groups (Abdallah and Ros, 2013). Isorhamnetin ($C_{16}H_{12}O_7$) is commonly found in yellow flowers. Endogenous Mexican plants such as *Tagetes lucida* flowers and *Opuntia ficus-indica* contain this flavonol among others. As a member of the flavonoids, the activity of the molecule depends on the functional groups available on the substitutions (Wang et al., 2018). It has been studied that isorhamnetin exhibits different biological activities such as anticoagulant (Ku et al., 2013a), anti-thrombotic (Ku et al., 2013b), antitumoral (Teng et al., 2006), and anti-inflammatory (Antunes-Ricardo et al., 2015). This work aims to evaluate the feasibility to use a microfluidic device as a mixer for the microencapsulation of isorhamnetin into biogenic silica from *Cyclotella* sp. for drug delivery applications.

2. Materials and methods

2.1. Chemicals and reagents

Isorhamnetin was purchased from Sigma-Aldrich, USA. SYLGARD silicone elastomer 184 and SYLGARD silicone elastomer 184 curing agent (Dow Corning Corporation, United States) was generously gifted by Dr. Sergio O. Martinez-Chapa from Tecnologico de Monterrey. All other chemicals and reagents were of analytical grade and were purchased from Sigma-Aldrich (United States).

2.2. Diatom cultivation

Cyclotella sp. was cultivated in a 500 mL non-agitated Erlenmeyer flask with 90 mL of Harrison's Artificial Seawater medium enriched with f/2 nutrients (Harrison et al., 1980) and 10 mL inoculum. The inoculum medium was comprised of: 347 mM NaCl, 23.8 mM Na_2SO_4, 7.68 mM KCl, 1.97 mM $NaHCO_3$, 690 μM KBr, 354 μM H_3BO_3, 63.3 μM NaF, 45.1 mM $MgCl_2{\cdot}6H_2O$, 8.74 mM $CaCl_2{\cdot}2H_2O$, and 78.0 μM $SrCl_2{\cdot}6H_2O$. The f/2 enrichment medium components consisted of 35.9 nM $Na_2MoO_4{\cdot}2H_2O$, 0.954 nM Na_2SeO_3, 6.0 nM $NiCl_2{\cdot}6H_2O$, 165 nM $ZnSO_4{\cdot}7H_2O$, 45.3 nM $CuSO_4{\cdot}5H_2O$, 24.7, nM $CoSO_4{\cdot}7H_2O$, 2.31 μM $MnSO_4{\cdot}4H_2O$, 19.7 μM $FeCl_3{\cdot}6H_2O$, and 21.9 μM ethylenedinitrol tetraacetic acid disodium salt ($C_{10}H_{14}O_8N_2Na_2{\cdot}2H_2O$). Vitamin solution consisted of 1.15 μM thiamine, 0.0005 nM biotin and 0.004 nM vitamin B12. The macronutrient medium consisted of 5.32 mM $NaNO_3$, 242 μM $NaH_2PO_4{\cdot}H_2O$ and 200 mM $Na_2SiO_3{\cdot}9H_2O$.

Culture media was sterilized by filtration using a 0.2 μm pore size filter (VWR Vacuum Filtration Systems, VWR, United States). Cultures were maintained at 22 °C, with a light intensity of 50 $\mu E/m^2s$, and a photoperiod of 14 h light and 10 h darkness. The cell suspension was subcultured every 3 weeks with 10% v/v inoculum. After three weeks, the flasks were gathered together in one sterile Erlenmeyer flask under similar conditions. Cell density and cell diameter were measured by triplicate using a cell counter (Z2 Coulter Particle Count and Size Analyzer, Beckman Coulter, United States) with a range of minimum threshold of 6 μm–19 μm. A dilution factor of 100 was used to measure cell density (100 μL cell suspension and 9.9 mL diluent).

A 5 L bubble column photobioreactor was used to study the growth kinetics of *Cyclotella* sp., characteristics and configuration mentioned elsewhere (Chiriboga and Rorrer, 2017). The culture media for the photobioreactor was the same as mentioned above, but changing the macronutrient solutions to 7 mM $NaNO_3$, 15 μM $NaH_2PO_4{\cdot}H_2O$ and 1 mM $Na_2SiO_3{\cdot}9H_2O$. The bubble column photobioreactor was initially inoculated with 60 mL cell suspension with a cell density of $1.06 \times 10^5 \pm 8.30 \times 10^3$ cells/mL. Filtered air and CO_2 were provided to the photobioreactor at a flow of 2.4 L/min, and 380 ppm respectively. Daily samples were taken to monitor cell density, pH and silicon concentrations in the reactor. Samples were taken by using a 60 mL sterile syringe with a withdrawn volume of 5 mL.

When the stationary phase was reached, the cell suspension was kept in starving conditions of two photoperiod cycles to synchronize all cells and to obtain a uniform material (Jeffryes et al., 2013). A centrifugation process was performed to harvest the diatoms by using 250 mL vessels and were centrifuged for 10 min at 1500 *g* (IEC CL30, Thermo Electron Corporation, United States). Dissolved silicon was measured by spectrophotometric assay: 5 mL of sample was mixed with 200 μL of 13% w/v ammonium molybdate solution in water, and 100 μL of 18.7% v/v hydrochloric acid (HCl). The reaction was left still for

10 min, 3 mL of the sample was transferred to a quartz cuvette and measured at 360 nm (Fanning and Pilson, 1973). Measurements were performed in duplicate. A dilution factor of 5 with distilled water was used when necessary. A standard curve of six points was done using Na_2SiO_3 as a standard.

2.3. Frustule isolation and preparation

Around, 115 mL of culture media with approximately 1×10^6 cells/mL was centrifuged at 1500 *g* for 15 min. Three washes with distilled water were performed. Cells were placed in a 50 mL centrifuge tube following the addition of 29.750 mL of 30% hydrogen peroxide (H_2O_2) and 250 µL of a 37% hydrochloric acid (HCl) solution. The mixture was inverted gently twice to allow the reagents mix with the cells. The centrifuge tube was placed in a vacuum for 1 h to eliminate bubbles. To avoid frustule breakage, the solution was maintained uncapped and without stirring for 42 h at room temperature (22 °C). The HCl/H_2O_2 solution was removed from the centrifuge tube using a pipette, 30 mL of distilled water was added, the mixture was inverted gently to wash cells, and left still for 6 h or until cells precipitated. Water washes were performed three times. Subsequently, frustules were washed 3 times with methanol to remove water (Jeffryes et al., 2008). Samples were kept in methanol under refrigeration (4 °C) until use.

2.4. Frustule characterization

Frustule characterization was performed using scanning electron microscope (SEM) (EVO MA25, Zeiss, United States). The sample was placed in the pin using carbon tape to adhere to the surface. One droplet of each sample was placed in the carbon tape and was let dried in a desiccator. 20 kV of voltage and variable pressure were used. The elemental analysis was determined with energy dispersive spectroscopy using a detector with a 20-kV accelerating voltage (Bruker XFlash 6/10, Bruker, United States). FT-IR spectroscopy was used to identify the typical bonds in the silica structure with a resolution of 4 cm^1 and range of 280–4000 cm^{-1} (Spectrum 400, PerkinElmer, United States).

2.5. Manufacturing of the microfluidic device

The microfluidic device was designed using AutoCAD software. The channels had a length of 500 µm and 1000 µm of height (Fig. 1). The device was designed with complex geometry with Y shape and 13 c-turns. The empty space between each channel is 1000 µm. The microfluidic mold was printed using a 3-D printer (Fortus 400mc, Proto3000, Canada) with acrylonitrile butadiene styrene (ABS) polymer. PDMS was used to manufacture the microfluidic device by using the ESCARGOT (Saggiomo and Velders, 2015). SYLGARD silicone elastomer 184 and SYLGARD silicone elastomer 184 curing agents were used to produce the PDMS in a ratio of 10:1 of sylgard 184: curing agent. A 3-D printed mold was placed in a glass container avoiding touching the base, then PDMS was poured into the glass container, and placed under vacuum in a desiccator to remove air bubbles for 1 h. The PDMS and the mold were cured for 2 h at 75 °C. After that, it was left in acetone for 12 h to dissolve the mold, after which microchannels were cleaned with acetone and dried passing air.

2.6. Isorhamnetin encapsulation

Three different flows (1600, 1000 and 500 µL/min) were used to regulate the residence time of frustules and drug inside de device (0.4 min, 1 min, and 2 min respectively), and three different drug concentrations (20 µg/mL, 60 µg/mL, and 100 µg/mL) were studied to determine the optimal drug encapsulation conditions. A design of experiments was performed to make the statistical analysis of the results. A multilevel factorial model (3^k) was used and analyzed with the Desing-Expert software (Version 11, State-Ease, Inc., United States). Encapsulated isorhamnetin concentration was calculated by absorbance as follow: samples were recollected from the microfluidic device outlet in a 2 mL Eppendorf tube. Samples were centrifuged at 13,000 rpm (Prism R, Labnet International, Inc., United States) for 10 min. The supernatant was discarded, and 1.5 mL of distilled water was added to remove non-adsorbed isorhamnetin. Samples were centrifuged at 13,000 rpm for 15 min, and the supernatant was removed with a glass Pasteur pipette. 1.5 mL acetone was added to each sample to desorb the isorhamnetin, samples were vortexed for 30 s, and centrifuged at 13,300 for 15 min. Approximately, 700 µL were placed in a quartz cuvette and absorbance was measured from 200 to 900 nm, where the highest peak was detected at 370 nm (DR5000, HACH, United States). Three standard curves of isorhamnetin in acetone were prepared in a range from 0.125 to 16 µg/mL. Encapsulation efficiency (EE%) and

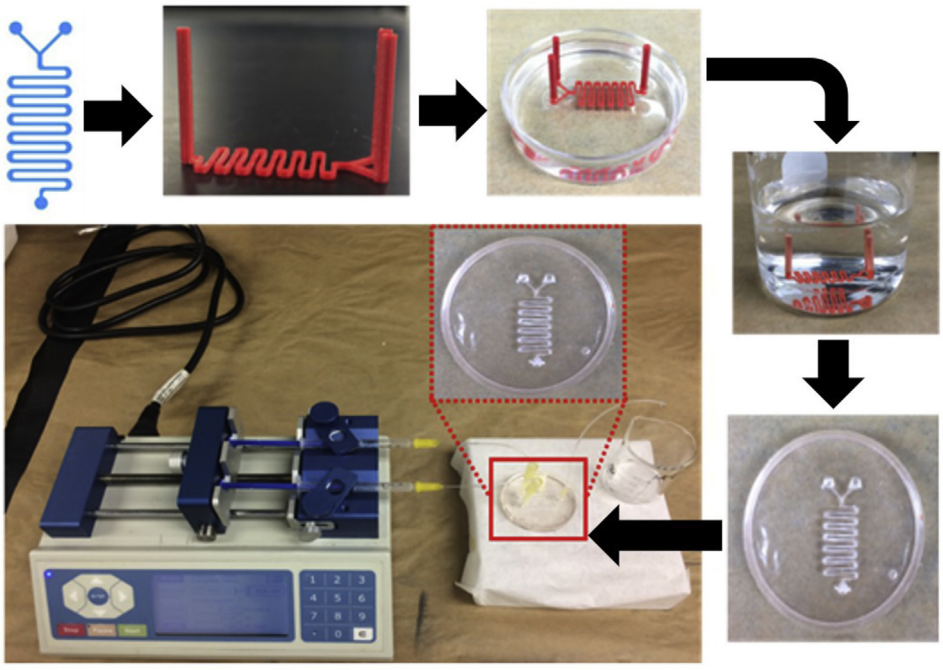

Fig. 1. Microfluidic device manufacturing. The design was performed in AutoCAD software with the following channels dimensions: 500 µm length and 1000 µm of height. The input and output points had a 1 mm diameter and 2 cm height. These were designed bigger due to tubing and manufacturing purposes. The design was printed in ABS polymer using a 3D printer followed by the pouring and curing the PDMS. Once the PDMS was cured, the ABS polymer was removed with acetone. The channels were cleaned with acetone, and the final configuration of the microfluidic device and the syringe pump is shown.

loading capacity were calculated according to the following equations:

$$EE\% = \left(\frac{Da - De}{Da}\right) * 100 \quad (3)$$

$$LC\ (\%) = \left(\frac{De}{F}\right) * 100 \quad (4)$$

Where

Da: mass of drug added (μg)
De: mass of entrapped drug (μg)
F: frustule weight per sample (μg)

2.7. Isorhamnetin release kinetics

Drug release kinetic experiments were performed using a simulated colonic fluid (SCF). The main components of SCF were 0.2 g/L potassium chloride, 8 g/L sodium chloride, 0.24 g/L potassium phosphate monobasic, 1.44 g/L sodium phosphate dibasic at pH 7 (Zhang et al., 2013). 30 mL of SCF were placed in a 125 mL Erlenmeyer flask and the samples. Flasks were maintained in agitation for 24 h, 37 °C, and 50 rpm. Sampling was performed every hour by taking 700 μL of sample, the same volume of SCF was added to maintain the same volume during the experiment. Isorhamnetin was measured spectrophotometrically with a range of 200–900 nm, where the highest peak was observed at 240 nm (DR5000, HACH, United States). A standard curve with isorhamnetin was done with 6 points with concentrations ranging from 0.031 to 8 μg/mL using as dissolvent SCF. All experiments were performed in duplicate.

3. Results and discussion

3.1. Diatom cultivation

Diatoms use dissolved silicon, in the form of silicic acid, to synthesize it into amorphous silica. Hence, silicon is the main factor that controls the division cell cycle. Fig. 2 shows the typical sigmoidal graphic for diatom cultivation. *Cyclotella* sp. was grown in a 5 L photobioreactor in an excess soluble medium to avoid cell stress (Jeffryes et al., 2013). In this study, diatoms exhibited a typical growth sigmoidal profile. A final cell density of 1.16×10^6 cells/mL was achieved after 87 h of cultivation. The maximum growth rate under the conditions mentioned was of 0.068 h^{-1} at 40 h. In comparison with other studies, the maximum growth achieved by *Cyclotella* sp. was 0.023 h^{-1} with perfusion of Si during semi-continuous cultivation (Jeffryes et al., 2013), and 1.45 d^{-1} with an initial Si concentration of 6.6 mg/L (Shafik et al., 1997). It has been studied that to achieve higher cell densities a multi-stage silicon addition where diatoms are cultivated in a silicon starvation phase and continue the second stage with a higher concentration of silicon. Additionally, a change in the light intensity and CO_2 to improve the photosynthesis assimilation was used (Ozkan and Rorrer, 2017).

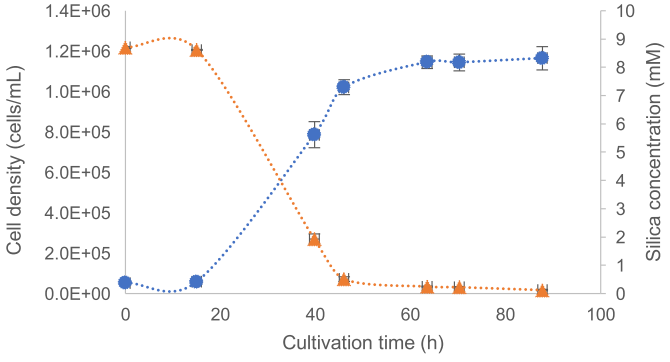

Fig. 2. *Cyclotella* sp. growth kinetics.

3.2. Frustule isolation and preparation

The organic material removal from frustules is a key component for the further applications such as carriers for medical applications where the frustule must be clean without losing the surface charge or biosensor for optical applications where the frustule has to be intact with no wrecks on the surface. Depending on the type of application, the methodology must be selected. Some methodologies can cause a change the softness or roughness of the structure, while others can modify the active groups in the surface. The hydrogen peroxide-hydrochloric acid (H_2O_2–HCl) through an oxidative reaction can remove most of the polysaccharides, proteins, and some metal ions on the structure; while producing a stiffer structure (Romann et al., 2016). SEM images showed an intact structure (Fig. 3A). Control sample consisted of the frustule with no treatment, it had all the organic material. Fractured structures were not observed; the complete valves were detected. Diatom cells had an average size of 10.96 ± 0.02 μm, the nanopores from the surface were measured at 180 nm on average. Both valves are connected through girdle bands which can be observed as horizontal circumferences (Fig. 3B).

According to the elemental analysis, frustules were composed of 30.53% silicon, 48.84% oxygen, and 20.63% carbon (Fig. 3C). According to literature, frustules are composed around 90% of silicon and other metals in trace amounts such as aluminum, iron, magnesium, titanium, sodium, phosphorus, manganese, potassium, chromium and calcium (Yuan et al., 2004; Gültürk and Güden, 2011). The FT-IR analysis was performed in a range of 4000–380 cm^{-1} (Fig. 3D). The typical peaks of Si–O–Si at 461 (bending), 796 (symmetric stretching) and 1100 (antisymmetric stretching) that corresponds to amorphous silica were observed. The crystallization of silica peak appears at 617 cm^{-1} (Gültürk and Güden, 2011), but in the current spectra, the peak is not shown indicating that the amorphous phase was kept during the acid cleaning methodology. The peak at 1632 cm^{-1} corresponded to deformation of an OH bending in water where Si–OH is included as well at the peak 3434 cm^{-1} (Jiang et al., 2014; Qi et al., 2017). The peak at 2919 cm^{-1} corresponded to alkanes (Gnanamoorthy et al., 2014). Depending on the resolution of the equipment and the cleaning methodology, usually with a thermal methodology, a peak from 3745 to 3750 cm^{-1} and peak at 3740 cm^{-1} can be observed individually and corresponds to isolated hydroxyl groups (Si–OH) OH vibration of silanol groups (Yuan et al., 2004).

3.3. Isorhamnetin encapsulation and SEM analysis

The encapsulation was performed by using a microfluidic device. Traditional methodologies involve the use of stirring and evaporation methods that can last several hours (Table 1). With this methodology, we expected to reduce the encapsulation time, while providing an efficient EE% and LC%. EE% describes the amount of drug that is encapsulated in the carrier in comparison with the initial drug concentration added. LC% indicates the mass percentage that corresponds to the drug in the total mass of the system (carrier and drug). The encapsulation was performed by adsorption on the surface. Therefore, the drug could be easily adsorbed or desorbed from the structure. By increasing the flow, the mixing between the drug and the frustules could have a higher diffusion rate. It is important to note that the diffusion rate is dependent on the solubility of the drug with the surface of the frustule.

The higher EE% was observed at 2 min as resident time and 20 μg/mL with a 17.92% followed by 16.40% (0.4 min, 20 μg/mL). According to the statistical analysis (data not shown), the interaction of the drug concentration and time resulted significant ($p < 0.05$) for entrapment efficiency. It can be observed that for the 100 μg/mL a range of 12–14% was obtained, while for 60 μg/mL the range observed was 9–14%

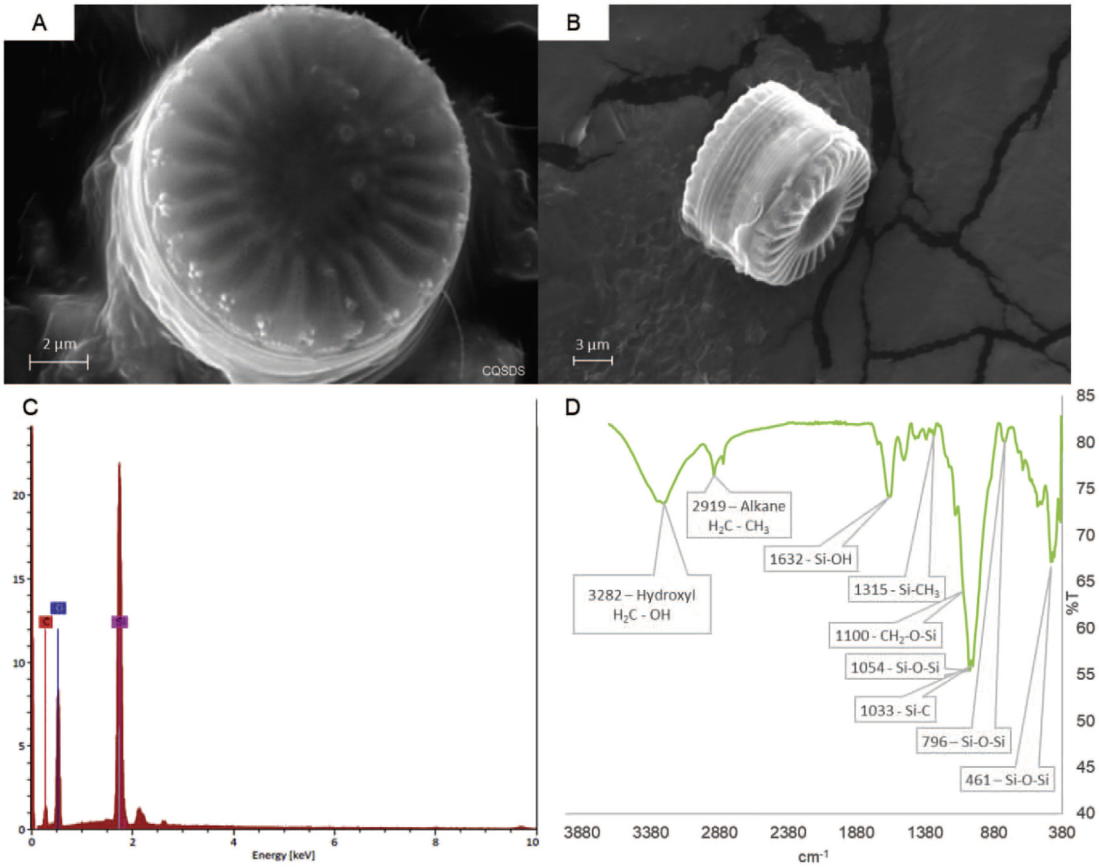

Fig. 3. *Cyclotella* sp. SEM images. A) Frontal view of the cell where the nanopores are seen. The bigger pores around the circumference corresponding to chitin fiber emerge points. B) Lateral view of the cell where the two valves are observed. C) Frustule elemental analysis. D) Typical FT-IR spectra of frustules.

(Fig. 4A). Isorhamnetin is a hydrophobic molecule while the surface of frustules has a hydrophilic. Hence, the low EE% can be attributed to the physicochemical characteristics of frustules and drug. Additionally, EE % depends on the surface area of the material, the porosity, and available functional groups in the surface (silanol, siloxane groups, or other functional groups added) (Izquierdo-Barba et al., 2005; Lim et al., 2015). However, other studies have reported the EE% in frustules from *Thalassiosira weissflogii* of 0.5% for frustules and 18% functionalized frustule (Cicco et al., 2015). In comparison with this report, the encapsulation efficiencies were similar but without the functionalization of the surface. Frustules from diatomaceous earth (DE) which are fossilized frustules, were found to reach 94% with no surface modification (Aw et al., 2012). As a continuation of the previous report, Aw et al., continued the investigation of 5 different types of surface functionalization methodologies and their effect on EE%; they found a range of 91–97% (Aw et al., 2013). Javalkote et al. (2015) compared the two encapsulation techniques of curcumin (flavonoid) to frustules from *Nitzschia* sp. The results exhibited 73% encapsulation for a non-magnetic frustule versus 41% and 49% for the two methodologies to produce magnetic particles and encapsulate flavonoid at the same time. Here the decrement of the EE% was due to the mass occupied by the magnetic molecule (Javalkote et al., 2015).

The loading capacity (LC%) showed an increment when the isorhamnetin concentration increased (Fig. 4B). The highest value obtained was 1.63% (2 min and 100 µg/mL) followed by 1.28 (0.4 min and 100 µg/mL). The interaction of all factors resulted significantly in the statistical analysis ($p < 0.05$). The optimum conditions to obtain the highest loading capacity was 2 min as residence time and 100 µg/mL. Similar results obtained with frustules obtained from *Thalassiosira weissflogii* with an LC% of 0.5% and 1.7% for functionalized frustules (Cicco et al., 2015). In this case, the encapsulation with the microfluidic device avoided the modification of the surface by achieving a similar result as the one reported from Cicco et al. However, other studies showed a higher LC% as in the case of the indomethacin drug (hydrophobic) encapsulation in a frustule of diatomaceous earth (DE) were 22% was reported (Aw et al., 2012). The same research group, in a further study, provided the information of functionalized DE with 5 types of functional groups and obtaining a range of 15–24% (Aw et al., 2013). Javalkote et al. (2015) reported the LC% 14.7% of a flavonoid in frustules, and 8.2 and 9.1% for encapsulation that involved the addition of magnetic material in addition to the flavonoid. Streptomycin was encapsulated in *Coscinodiscus concinnus* frustules by a drop-wise loading methodology achieving a loading capacity of 33.33% (Gnanamoorthy et al., 2014). A comparison between the present study and the literature is presented (Table 1). As previously discussed, the main differences of the LC% are related to the surface and drug characteristics and compatibility among them. Additionally, in the traditional methodologies, turbulent flows are produced due to the stirring of the drug in solution and frustules. In comparison, in a microfluidic device, the laminar flow in the microchannels may not be enough to create the optimum mixing conditions. The adsorption of biomolecules to frustules relies on the electrostatic interactions, van der Waals forces, and/or hydrophobic interactions (Abdallah and Ros, 2013). For hydrophobic drugs, it has been reported the addition of functional groups to produce a hydrophobic surface. In this case, the problem of having a hydrophilic surface and hydrophobic drug can be minimized, and the encapsulation efficiency and loading capacity can be maximized. In addition, the attachment of specific functional groups can improve the EE% and LC% due to covalent bonding. SEM images of isorhamnetin encapsulation are shown (Fig. 5). The brighter points in the surface corresponded to isorhamnetin attached to the surface. A uniform encapsulation was not observed, but rather a heterogeneous dispersion of the flavonoid. This

Table 1
Comparison of EE% and LC% between frustules obtained from different diatom. SF: surface functionalization, ET: encapsulation time, + more than that number of hours.

Marine organism	Frustule size	Frustule shape	Drug	Drug nature	Encapsulation technique	SF	ET	%EE	%LC	Reference
Cyclotella sp.	10.96 ± 0.02 µm	Centric	Isorhamnetin	Hydrophobic	Microfluidic device	No	2 min	17.92%	1.63%	Present work
Thalassiosira weissflogii	10–15 µm	Centric	Ciprofloxacin	Hydrophobic	Stirring at 37 °C	No	4 h	6%	0.5%	Dong and Mumper (2010)
Thalassiosira weissflogii	10–15 µm	Centric	Ciprofloxacin	Hydrophobic	Stirring at 37 °C	Yes	4 h	18%	1.7%	Dong and Mumper (2010)
Nitzschia sp.	8 µm	Pennate	Curcumin	Hydrophobic	Stirring	No	5 h	73%	14.7%	Hashemipour and Panahi (2017)
Nitzschia sp.	8 µm	Pennate	Curcumin	Hydrophobic	Ferrofluid technique	No	5 h	41%	8.2%	Hashemipour and Panahi (2017)
Nitzschia sp.	8 µm	Pennate	Curcumin	Hydrophobic	In situ technique	No	5 h	49%	9.1%	Hashemipour and Panahi (2017)
Diatomaceous earth (DE) Aulacoseira sp.	4–6 µm diameter, 10–20 µm length	Centric	Indomethacin	Hydrophobic	Drop-wise loading	No	+3 h	94%	22%	Logie et al. (2017)
Diatomaceous earth (DE) Aulacoseira sp.	4–6 µm diameter, 10–20 µm length	Centric	Indomethacin	Hydrophobic	Drop-wise loading	Yes	+2 h	91–97%	15–24%	Joseph (2018)
Coscinodiscus concinnus	220 µm	Centric	Streptomycin	Hydrophilic	Drop-wise loading	No	+3 h	–	33.3%	Liang et al. (2017)

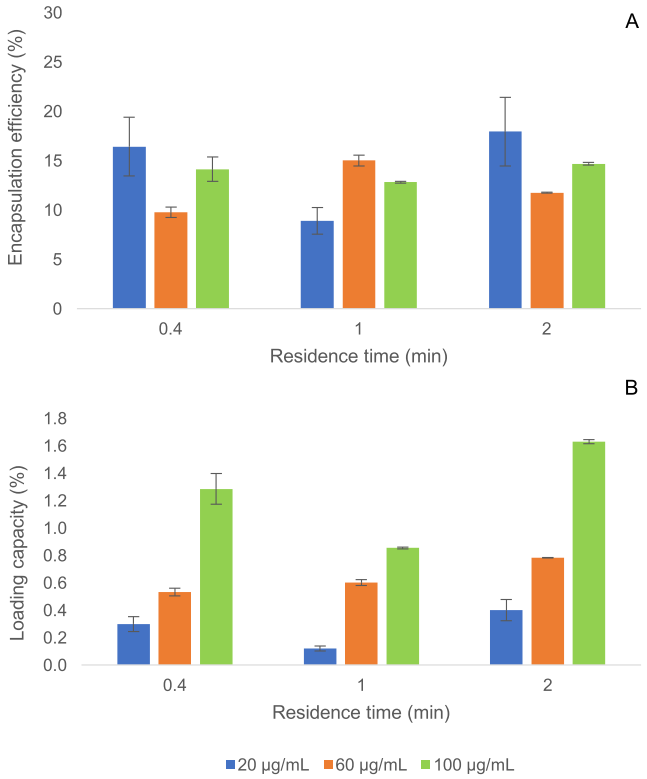

Fig. 4. A) Encapsulation efficiency (%), B) Loading capacity. In both graphics, three drug concentrations were used (20,60 and 100 µg/mL) and three residence time (0.4, 1 and 2 min). Error bars represent the standard deviation of triplicates.

can be attributed to the low intramolecular interactions between the flavonoid and the available functional groups in the silica surface.

3.4. Isorhamnetin release kinetics

Once the statistical analysis and optimum conditions of encapsulation were obtained, the encapsulation was performed with the optimum conditions (2 min and 20 µg/mL) for the study of drug release. Drug release studies were performed in a simulated colonic fluid at 37 °C. A burst release in the first hour of the study achieving 48.26% was observed (Fig. 6). The total release was accomplished after 3 h of the study. Since the flavonoid was attached to the surface, the release was faster in comparison with the drug that may be attached covalently to a specific functional group. When the drug is placed in the inner pores of the frustule, the release rate from it can be reduced due to the intramolecular interactions between the flavonoid and the silica (Stewart et al., 2018). It is worth noting that the release rate depends on the nature of the medium, ionic strength of the surface and the drug, and pH (Stewart et al., 2018). The hydrophobic state of the medium could have retained the release of the flavonoid from the surface; however, due to the low EE% obtained, the drug could have been more prone to be desorbed. Javalkote et al. (2015) reported the total release of the curcumin after 12 h of the analysis. Several studies reported by using a covalent attachment of the drug to the frustule surface showed a slower and sustained release of the drug of 7 days (Cicco et al., 2015), and 14 days (Aw et al., 2013). It has been studied the isorhamnetin pharmacokinetics in beagle dogs and rats. It was found a half-life ($t_{1/2}$) of 5.4 h for beagle dogs and 5.7 h for rats, while the time to reach maximum isorhamnetin concentrations in plasma were (T_{max}) 2.6 h for beagle dogs, and 6.4–7.21 h for rats (Chen et al., 2010; Zhao et al., 2013; Duan et al., 2016). For this study, the drug release in 3 h could represent at least 8 h of therapeutic effect in plasma due to the protection effect that

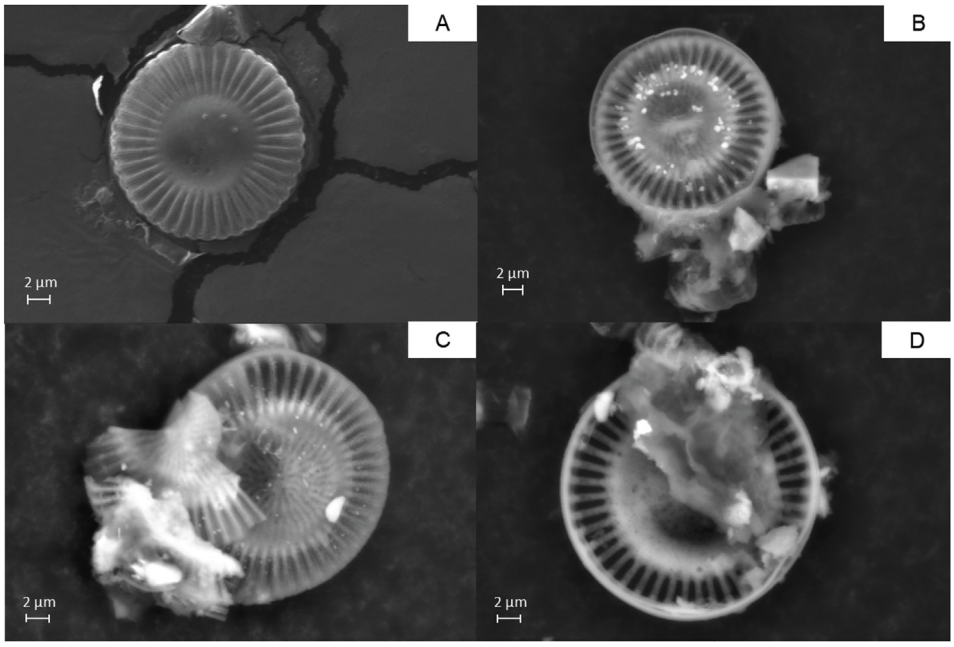

Fig. 5. Isorhamnetin encapsulation in different concentrations in *Cyclotella quillensis* frustules. A) Control, B) 20 µg/mL, C) B) 60 µg/mL and D) B) 100 µg/mL.

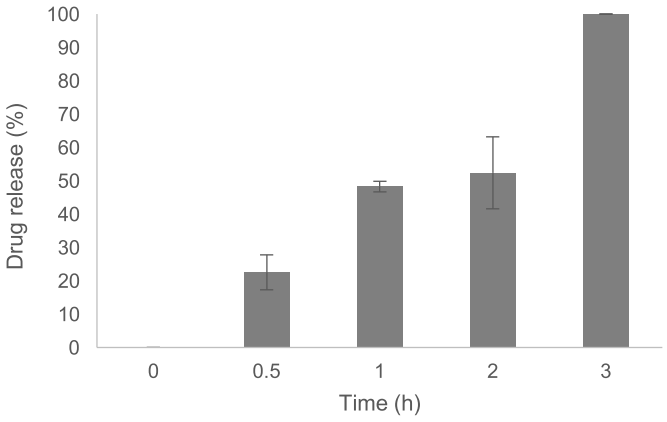

Fig. 6. Percent drug release. Bars represent the standard deviation of triplicates.

the frustule provides to the drug.

4. Conclusion

This study reported the use of biogenic silica (frustules) obtained from diatom microalgae to explore their use as a carrier for drug delivery. The *Cyclotella* sp. cultivation in photobioreactors allowed to obtain a considerable amount of biomass. SEM and FT-IR analysis techniques allowed the successful characterization of the frustules and the encapsulated isorhamnetin into frustules. ESCARGOT methodology represented a cheap, easy and functional methodology to manufacture microfluidic devices. A novel encapsulation methodology using a microfluidic device was used to compare its encapsulation efficiency (EE %) with traditional methodologies. This methodology allowed to perform faster encapsulation processes that were performed in minutes compared with hours from traditional methodologies. The rich OH groups available in frustules were responsible for the encapsulation through intramolecular interactions. The highest EE% and LC% were 17.92% and 1.63% respectively. The optimal conditions for encapsulation were 2 min as resident time in the microfluidic device and an isorhamnetin concentration of 20 µg/mL. Drug release behavior in a simulated fluid was observed to have a burst release in the first hour by releasing 48.26% of the drug. The total amount of isorhamnetin was release in 3 h. The hypotheses of this work were developed and successfully addressed.

Conflicts of interest

The authors report no conflicting interest in any capacity, competing or financial.

Acknowledgments

Authors are grateful to the School of Chemical, Biological, and Environmental Engineering at Oregon State University, Centro del Agua and Centro de Biotecnología FEMSA from Tecnologico de Monterrey for providing research facilities and technical support. The financial support provided by the Emerging Technologies and Molecular Nutrition Research Group from Tecnologico de Monterrey and Consejo Nacional de Ciencia y Tecnologia (CONACYT), Mexico is thankfully acknowledged. The first author, “Elena I. Mancera-Andrade” thankfully acknowledge the Master Scholarship (No. 446209) awarded by Consejo Nacional de Ciencia y Tecnologia (CONACYT), Mexico.

References

Abdallah, B.G., Ros, A., 2013. Surface coatings for microfluidic-based biomedical devices. In: Microfluidic Devices for Biomedical Applications. Woodhead Publishing, pp. 63–99.

Ahmed, I., Akram, Z., Bule, M., Iqbal, H., 2018a. Advancements and potential applications of microfluidic approaches—a review. Chemosensors 6 (4), 46.

Ahmed, I., Iqbal, H.M., Akram, Z., 2018b. Microfluidics engineering: recent trends, valorization, and applications. Arabian J. Sci. Eng. 43 (1), 23–32.

Amreddy, N., Babu, A., Panneerselvam, J., Srivastava, A., Muralidharan, R., Chen, A.,, et al., 2018. Chemo-biologic combinatorial drug delivery using folate receptor-targeted dendrimer nanoparticles for lung cancer treatment. Nanomed. Nanotechnol. Biol. Med. 14 (2), 373–384.

Antunes-Ricardo, M., Gutiérrez-Uribe, J.A., López-Pacheco, F., Alvarez, M.M., Serna-Saldivar, S.O., 2015. In vivo anti-inflammatory effects of isorhamnetin glycosides isolated from Opuntia ficus-indica (L.) Mill cladodes. Ind. Crops Prod. 76, 803–808.

Aw, M.S., Bariana, M., Yu, Y., Addai-Mensah, J., Losic, D., 2013. Surface-functionalized diatom microcapsules for drug delivery of water-insoluble drugs. J. Biomater. Appl. 28 (2), 163–174.

Aw, M.S., Simovic, S., Yu, Y., Addai-Mensah, J., Losic, D., 2012. Porous silica microshells from diatoms as biocarrier for drug delivery applications. Powder Technol. 223,

52–58.
Barsanti, L., Gualtieri, P., 2014. Algae: Anatomy, Biochemistry, and Biotechnology. CRC press, pp. 221–266.
Chen, Z.P., Sun, J., Chen, H.X., Xiao, Y.Y., Liu, D., Chen, J.,, et al., 2010. Comparative pharmacokinetics and bioavailability studies of quercetin, kaempferol and isorhamnetin after oral administration of Ginkgo biloba extracts, Ginkgo biloba extract phospholipid complexes and Ginkgo biloba extract solid dispersions in rats. Fitoterapia 81 (8), 1045–1052.
Chiriboga N, O.G., Rorrer, G.L., 2017. Control of chitin nanofiber production by the lipid-producing diatom Cyclotella Sp. through fed-batch addition of dissolved silicon and nitrate in a bubble-column photobioreactor. Biotechnol. Prog. 33 (2), 407–415.
Cicco, S.R., Vona, D., De Giglio, E., Cometa, S., Mattioli-Belmonte, M., Palumbo, F.,, et al., 2015. Chemically modified diatoms biosilica for bone cell growth with combined drug-delivery and antioxidant properties. ChemPlusChem 80 (7), 1104–1112.
de Jesús Rostro-Alanis, M., Mancera-Andrade, E.I., Patiño, M.B.G., Arrieta-Baez, D., Cardenas, B., Martinez-Chapa, S.O., Saldívar, R.P., 2016. Nanobiocatalysis: nanostructured materials–a minireview. Biocatalysis 2 (1), 1–24.
Diab, R., Canilho, N., Pavel, I.A., Haffner, F.B., Girardon, M., Pasc, A., 2017. Silica-based systems for oral delivery of drugs, macromolecules and cells. Adv. Colloid Interface Sci. 249, 346–362.
Dong, X., Mumper, R.J., 2010. Nanomedicinal strategies to treat multidrug-resistant tumors: current progress. Nanomedicine 5 (4), 597–615.
Duan, J., Dang, Y., Meng, H., Wang, H., Ma, P., Li, G.,, et al., 2016. A comparison of the pharmacokinetics of three different preparations of total flavones of Hippophae rhamnoides in beagle dogs after oral administration. Eur. J. Drug Metab. Pharmacokinet. 41 (3), 239–249.
Fanning, K.A., Pilson, M., 1973. On the spectrophotometric determination of dissolved silica in natural waters. Anal. Chem. 45 (1), 136–140.
Fonseca, A.C., Serra, A.C., Coelho, J.F., 2015. Bioabsorbable polymers in cancer therapy: latest developments. EPMA J. 6 (1), 22.
Gnanamoorthy, P., Anandhan, S., Prabu, V.A., 2014. Natural nanoporous silica frustules from marine diatom as a biocarrier for drug delivery. J. Porous Mater. 21 (5), 789–796.
Graves, R.A., Ledet, G.A., Glotser, E.Y., Mitchner, D.M., Bostanian, L.A., Mandal, T.K., 2015. Formulation and evaluation of biodegradable nanoparticles for the oral delivery of fenretinide. Eur. J. Pharm. Sci. 76, 1–9.
Gültürk, E., Güden, M., 2011. Thermal and acid treatment of diatom frustules. J. Achiev. Mater. Manuf. Eng. 46, 196–203.
Hans, M.L., Lowman, A.M., 2002. Biodegradable nanoparticles for drug delivery and targeting. Curr. Opin. Solid State Mater. Sci. 6 (4), 319–327.
Harrison, P.J., Waters, R.E., Taylor, F.J.R., 1980. A broad spectrum artificial sea water medium for coastal and open ocean phytoplankton 1. J. Phycol. 16 (1), 28–35.
Hashemipour, S., Panahi, H.A., 2017. Fabrication of magnetite nanoparticles modified with copper based metal organic framework for drug delivery system of letrozole. J. Mol. Liq. 243, 102–107.
Iqbal, H.M., Keshavarz, T., 2018. Bioinspired polymeric carriers for drug delivery applications. In: Stimuli Responsive Polymeric Nanocarriers for Drug Delivery Applications, vol. 1. pp. 377–404.
Izquierdo-Barba, I., Martinez, Á., Doadrio, A.L., Pérez-Pariente, J., Vallet-Regí, M., 2005. Release evaluation of drugs from ordered three-dimensional silica structures. Eur. J. Pharm. Sci. 26 (5), 365–373.
Javalkote, V.S., Pandey, A.P., Puranik, P.R., Deshmukh, P.K., 2015. Magnetically responsive siliceous frustules for efficient chemotherapy. Mater. Sci. Eng. C 50, 107–116.
Jeffryes, C., Gutu, T., Jiao, J., Rorrer, G.L., 2008. Two-stage photobioreactor process for the metabolic insertion of nanostructured germanium into the silica microstructure of the diatom Pinnularia sp. Mater. Sci. Eng. C 28 (1), 107–118.
Jeffryes, C., Rosenberger, J., Rorrer, G.L., 2013. Fed-batch cultivation and bioprocess modeling of Cyclotella sp. for enhanced fatty acid production by controlled silicon limitation. Algal Research 2 (1), 16–27.
Jiang, W., Luo, S., Liu, P., Deng, X., Jing, Y., Bai, C., Li, J., 2014. Purification of biosilica from living diatoms by a two-step acid cleaning and baking method. J. Appl. Phycol. 26 (3), 1511–1518.
Joseph, J., 2018. Experimental optimization of Lornoxicam liposomes for sustained topical delivery. Eur. J. Pharm. Sci. 112, 38–51.
Khan, I.U., Serra, C.A., Anton, N., Vandamme, T., 2013. Microfluidics: a focus on improved cancer targeted drug delivery systems. J. Control. Release 172 (3), 1065–1074.
Ku, S.K., Kim, T.H., Bae, J.S., 2013a. Anticoagulant activities of persicarin and isorhamnetin. Vasc. Pharmacol. 58 (4), 272–279.
Ku, S.K., Kim, T.H., Lee, S., Kim, S.M., Bae, J.S., 2013b. Antithrombotic and profibrinolytic activities of isorhamnetin-3-O-galactoside and hyperoside. Food Chem. Toxicol. 53, 197–204.
Kumar, S., Malik, M.M., Purohit, R., 2017. Synthesis methods of mesoporous silica materials. Mater. Today: Proceedings 4 (2), 350–357.
Liang, L., Shen, J.W., Wang, Q., 2017. Molecular dynamics study on DNA nanotubes as drug delivery vehicle for anticancer drugs. Colloids Surfaces B Biointerfaces 153, 168–173.
Lim, G.W., Lim, J.K., Ahmad, A.L., Chan, D.J.C., 2015. Influences of diatom frustule morphologies on protein adsorption behavior. J. Appl. Phycol. 27 (2), 763–775.
Logie, J., Ganesh, A.N., Aman, A.M., Al-awar, R.S., Shoichet, M.S., 2017. Preclinical evaluation of taxane-binding peptide-modified polymeric micelles loaded with docetaxel in an orthotopic breast cancer mouse model. Biomaterials 123, 39–47.
Mancera-Andrade, E.I., Parsaeimehr, A., Arevalo-Gallegos, A., Ascencio-Favela, G., Parra Saldivar, R., 2018. Microfluidics technology for drug delivery: a review. Front. Biosci. (Elite Ed.) 10, 74–91.
Napierska, D., Thomassen, L.C., Lison, D., Martens, J.A., Hoet, P.H., 2010. The nanosilica hazard: another variable entity. Part. Fibre Toxicol. 7 (1), 39.
Ozkan, A., Rorrer, G.L., 2017. Lipid and chitin nanofiber production during cultivation of the marine diatom Cyclotella sp. to high cell density with multistage addition of silicon and nitrate. J. Appl. Phycol. 29 (4), 1811–1818.
Qi, Y., Wang, X., Cheng, J.J., 2017. Preparation and characteristics of biosilica derived from marine diatom biomass of Nitzschia closterium and Thalassiosira. Chin. J. Oceanol. Limnol. 35 (3), 668–680.
Rasheed, T., Bilal, M., Abu-Thabit, N.Y., Iqbal, H.M., 2018. The smart chemistry of stimuli-responsive polymeric carriers for target drug delivery applications. In: Stimuli Responsive Polymeric Nanocarriers for Drug Delivery Applications, vol. 1. pp. 61–99.
Raza, A., Hayat, U., Rasheed, T., Bilal, M., Iqbal, H.M., 2019a. “Smart” materials-based near-infrared light-responsive drug delivery systems for cancer treatment: a review. J. Mater. Res. Technol. 8, 1497–1509.
Raza, A., Rasheed, T., Nabeel, F., Hayat, U., Bilal, M., Iqbal, H., 2019b. Endogenous and exogenous stimuli-responsive drug delivery systems for programmed site-specific release. Molecules 24 (6), 1117.
Romann, J., Chauton, M.S., Hanetho, S.M., Vebner, M., Heldal, M., Thaulow, C.,, et al., 2016. Diatom frustules as a biomaterial: effects of chemical treatment on organic material removal and mechanical properties in cleaned frustules from two Coscinodiscus species. J. Porous Mater. 23 (4), 905–910.
Ruiz-Ruiz, F., Mancera-Andrade, E.I., Parra-Saldivar, R., Keshavarz, T., Iqbal, H., 2017. Drug delivery and cosmeceutical applications of poly-lactic acid based novel constructs-A review. Curr. Drug Metabol. 18 (10), 914–925.
Saggiomo, V., Velders, A.H., 2015. Simple 3D printed scaffold-removal method for the fabrication of intricate microfluidic devices. Adv. Sci. 2 (9), 1500125.
Schultz, H.B., Thomas, N., Rao, S., Prestidge, C.A., 2018. Supersaturated silica-lipid hybrids (super-SLH): an improved solid-state lipid-based oral drug delivery system with enhanced drug loading. Eur. J. Pharm. Biopharm. 125, 13–20.
Shafik, H.M., Herodek, S., Vörös, L., Presing, M., Kiss, K.T., 1997. Growth of Cyclotella meneghiniana Kutz. I. Effects of temperature, light and low rate of nutrient supply. In: Annales de Limnologie-International Journal of Limnology, vol. 33. pp. 139–147.
Sosa-Hernández, J., Villalba-Rodríguez, A., Romero-Castillo, K., Aguilar-Aguila-Isaías, M., García-Reyes, I., Hernández-Antonio, A.,, et al., 2018. Organs-on-a-Chip module: a review from the development and applications perspective. Micromachines 9 (10), 536.
Stewart, C.A., Finer, Y., Hatton, B.D., 2018. Drug self-assembly for synthesis of highly-loaded antimicrobial drug-silica particles. Sci. Rep. 8 (1), 895.
Teng, B.S., Lu, Y.H., Wang, Z.T., Tao, X.Y., Wei, D.Z., 2006. In vitro anti-tumor activity of isorhamnetin isolated from Hippophae rhamnoides L. against BEL-7402 cells. Pharmacol. Res. 54 (3), 186–194.
Tian, P., Guo, Z., 2017. Bioinspired silica-based superhydrophobic materials. Appl. Surf. Sci. 426, 1–18.
Vishnubhakthula, S., Elupula, R., Durán-Lara, E.F., 2017. Recent advances in hydrogel-based drug delivery for melanoma cancer therapy: a mini review. J. Drug Deliv. 2017 Article ID 7275985, 9 pages. https://doi.org/10.1155/2017/7275985.
Wang, T.Y., Li, Q., Bi, K.S., 2018. Bioactive flavonoids in medicinal plants: structure, activity and biological fate. Asian J. Pharm. Sci. 13 (1), 12–23.
Xin, Y., Huang, Q., Tang, J.Q., Hou, X.Y., Zhang, P., Zhang, L.Z., Jiang, G., 2016. Nanoscale drug delivery for targeted chemotherapy. Cancer Lett. 379 (1), 24–31.
Yuan, P., Wu, D.Q., He, H.P., Lin, Z.Y., 2004. The hydroxyl species and acid sites on diatomite surface: a combined IR and Raman study. Appl. Surf. Sci. 227 (1–4), 30–39.
Zhang, D., Wang, Y., Cai, J., Pan, J., Jiang, X., Jiang, Y., 2012. Bio-manufacturing technology based on diatom micro-and nanostructure. Chin. Sci. Bull. 57 (30), 3836–3849.
Zhang, H., Shahbazi, M.A., Mäkilä, E.M., da Silva, T.H., Reis, R.L., Salonen, J.J., et al., 2013. Diatom silica microparticles for sustained release and permeation enhancement following oral delivery of prednisone and mesalamine. Biomaterials 34 (36), 9210–9219.
Zhao, G., Duan, J., Xie, Y., Lin, G., Luo, H., Li, G., Yuan, X., 2013. Effects of solid dispersion and self-emulsifying formulations on the solubility, dissolution, permeability and pharmacokinetics of isorhamnetin, quercetin and kaempferol in total flavones of Hippophae rhamnoides L. Drug Dev. Ind. Pharm. 39 (7), 1037–1045.